The present and future of numerical simulation techniques for off-shell science

M. Ohtsu

Research Origin for Dressed Photon,

3-13-19 Moriya-cho, Kanagawa-ku, Yokohama, Kanagawa 221-0022 Japan

Abstract

The first part of this article presents experimental results on novel devices that were fabricated and operated by utilizing dressed photons. The fabricated devices were photovoltaic devices having an Ag-electrode with a unique surface morphology, light-emitting diodes using silicon crystals, and nano-droplets in which pairs of nanometer-sized semiconductor particles were confined. The second part reviews the results of the numerical simulations for these devices using a random walk model. This model relies on statistical mechanics and complex-systems science. The third part describes the problems with these simulations and presents some suggestions for solving them. Finally, the need for a three-dimensional off-shell scientific model that takes account of interactions in a nanometric space is pointed out.

1. Introduction

The dressed photon (DP) is a quantum field that is created as a result of interactions among photons, electrons (excitons), and phonons in a nanometric space. The DP has been intensively studied as a representative topic of off-shell science [1-3]. Novel theories of the DP have been developed and used as a guide to support experimental studies, including a variety of advanced technologies [1].

A principal difficulty of developing these theories is that the size of the DP is much smaller than the wavelength of light. This means that the electromagnetic modes of the DP cannot be defined by the theories of conventional optical science (on-shell science). In order to overcome this difficulty, the DP has been expressed as a superposition of an infinite number of electromagnetic modes in the on-shell region, which allowed derivation of creation and annihilation operators for the DP. The operators representing the coupled state of a DP and phonons were also derived. Furthermore, theoretical analysis of a microscopic system surrounded by a macroscopic system yielded a Yukawa-type function for representing the spatially localized nature of the DP energy.

After this, the remaining theoretical problem to be solved was how to describe the autonomy observed in DP energy transfer and its measurement process [1,4]. For this description,

numerical simulations have been carried out by using a random walk model relying on statistical mechanics and complex-systems science.

Section 2 of this article reviews experimental results that have been reproduced by numerical simulations. Section 3 reviews the results of these simulations and presents the problems associated with them. Section 4 presents possible directions for solving these problems, which could promote advances in off-shell science. Section 5 presents a summary of this article.

2. Experimental results for novel devices fabricated and operated based on dressed photons

This section reviews experimental results for three novel devices that have been fabricated and operated by using DPs.

2.1 Photovoltaic devices having a silver electrode with a unique surface morphology

Photovoltaic devices convert optical energy to electrical energy and have been used as solar cell batteries. Here, a device using organic molecules of poly(3-hexylthiophene) (P3HT) are reviewed as an example. Autonomously created DPs were utilized for fabrication and operation of this device in order to realize a high conversion efficiency. The details of the fabrication and operation have been described in [5]. They can be summarized as follows:

Fabrication

A P3HT film was used as a p-type semiconductor having a bandgap energy, E_g, of 2.18 eV, and therefore, the cutoff-wavelength, λ_c, for optical to electrical energy conversion was 570 nm. A ZnO film was used as an n-type semiconductor (E_g=3.37 eV, λ_c=367 nm). A transparent ITO film and an Ag film were used as two electrodes. The principal features of this photovoltaic device originated from the P3HT because a depletion layer of the pn-junction was formed inside the P3HT. Films of ITO, ZnO, P3HT, and Ag were deposited successively on a sapphire substrate to thicknesses of 200 nm, 100 nm, 50 nm, and several nm, respectively, in order to make a preliminary device (Fig. 1).

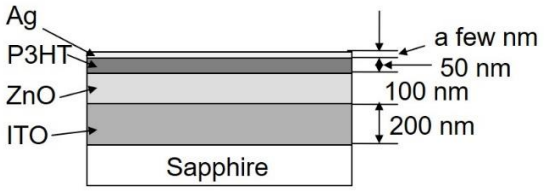

Fig. 1 Preliminary photovoltaic device using an Ag film as an electrode.

On the Ag film of the preliminary device, Ag particles were deposited by the method shown in Fig. 2: While Ag particles were being deposited by RF-sputtering, the surface of the Ag film was irradiated with light to create DPs, and a reverse bias voltage, V_b, was applied to the pn-junction. Here, the wavelength λ_0 of the irradiation light was longer than λ_c. As an example, λ_0 was set to 660 nm, and V_b was -1.5 V.

The fabrication principle was such that the autonomously created DPs and the reverse bias voltage controlled the amount of Ag particles that flew into and out of the Ag film surface. The fabrication process was as follows:

(1) Creation of electron–hole pairs by the DPs (Fig. 3(a)): The DPs were created at bumps on the Ag film surface by the irradiation light. If the field of the DPs extended to the pn-junction, electrons were excited to create electron–hole pairs even though the photon energy of the irradiation light was lower than E_g. This unique excitation was possible due to the contribution of the energy of the phonon that was a constituent element of the DP.

(2) Charging the Ag film (Fig. 3(b)): The created electron–hole pairs were annihilated by the electric field generated by the reverse bias voltage, and the positive holes were attracted to the Ag film electrode. As a result, the Ag film was positively charged.

(3) Autonomous control of Ag particle deposition (Fig. 3(c)): The Ag particles striking the Ag film surface were positively charged because they passed through an Ar plasma for RF-sputtering. Therefore, these Ag particles were repulsed from the area of the Ag film surface that was locally positively charged as a result of efficient creation of DPs in steps **(1)** and **(2)**. As a result, the repulsed Ag particles were deposited on other areas of the Ag film surface.

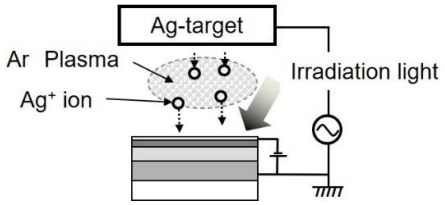

Fig. 2 Deposition of Ag particles by RF-sputtering under light irradiation.

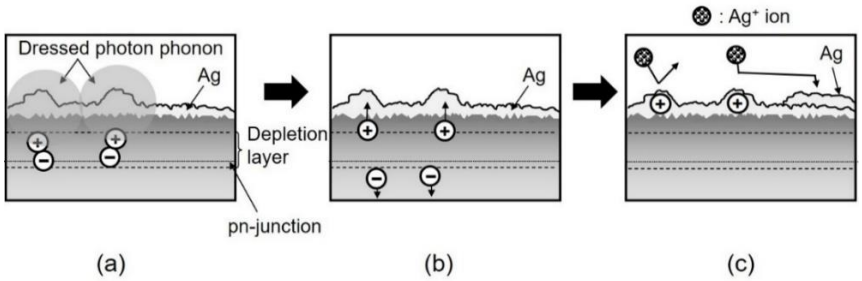

Fig. 3 Principle of controlling the amount of Ag particles that flew into and out of the Ag film surface.
(a), (b), (c) represent the creation of electron-hole pairs by the DP, charging of the Ag film, and autonomous control of the Ag particle deposition, respectively.

By steps **(1)**–**(3)**, a unique surface morphology was formed on the Ag film, which was governed by the spatial distribution of the DPs. The fabrication process finished autonomously once the spatial distribution of the created DPs reached a stationary state.

Table 1 summarizes the values of the irradiation light power, P, and the reverse bias voltage, V_b, for three devices A, B, and C. Figure 4 shows scanning electron microscope (SEM) images of the Ag film surfaces. The images show that the surfaces of devices B and C (Fig. 4(b) and (c)) were rougher than that of device A (Fig. 4(a)) due to the larger Ag grains grown on the surface. The lower parts in Figs. 4(b) and (c) show histograms of the distribution of grain diameters, derived by assuming spherical grain shapes. The solid curves are lognormal functions fitted to these histograms. In Fig. 4(b), the average and the standard deviation of the diameter were 90 nm and 64 nm, respectively, whereas they were respectively 86 nm and 32 nm in Fig. 4(c). By comparing these values, it was found that the standard deviation decreased with increasing light power, P, which meant that a surface morphology with unique-sized grains was autonomously formed due to the high irradiation power. A unique feature of the histograms in Figs. 4(b) and (c) was the bumps, identified by downward arrows, that deviated from the lognormal functions.

Table 1 The values of the irradiation light power, P, and the reverse bias voltage, V_b, for device fabrication.

Name of device	Irradiation light power, P	Reverse bias voltage, V_b
A(1)	0	0
B	50 mW	-1.5 V
C	70 mW	-1.5 V

(1) A is a reference device that was fabricated to compare its performance with that of devices B and C.

Operation

To operate the device fabricated above, it was irradiated with light from the rear surface of the sapphire substrate (Fig. 5). Since the spatial distributions of the DPs created on the Ag grains in Figs. 4(b) and (c) depended on the grain sizes (the average diameters of the grains were 90 nm and 86 nm, respectively), the DP fields of devices B and C extended to the pn-junctions because the sum of the thicknesses of the Ag film and the P3HT was less than 70 nm. As a result, electron–hole pairs were created by these DPs when the device was irradiated with light*. Even though the photon energy of the irradiation light was lower than E_g, optical to electrical energy up-conversion was expected thanks to the energy of the phonons, constituent elements of the DP. Furthermore, it was expected that the efficiency of creating the electron–hole pairs would be highest when the irradiation light wavelength was equal to the wavelength, λ_0, of the light irradiated during the

fabrication process. This phenomenon is called the photon breeding (PB) effect [6], and will be reviewed also in Section 2.2.

(*) In the case of device A, on the other hand, the field of the DPs did not reach the pn-junction because the Ag film was too thick (800 nm) to allow electron–hole pairs to be created.

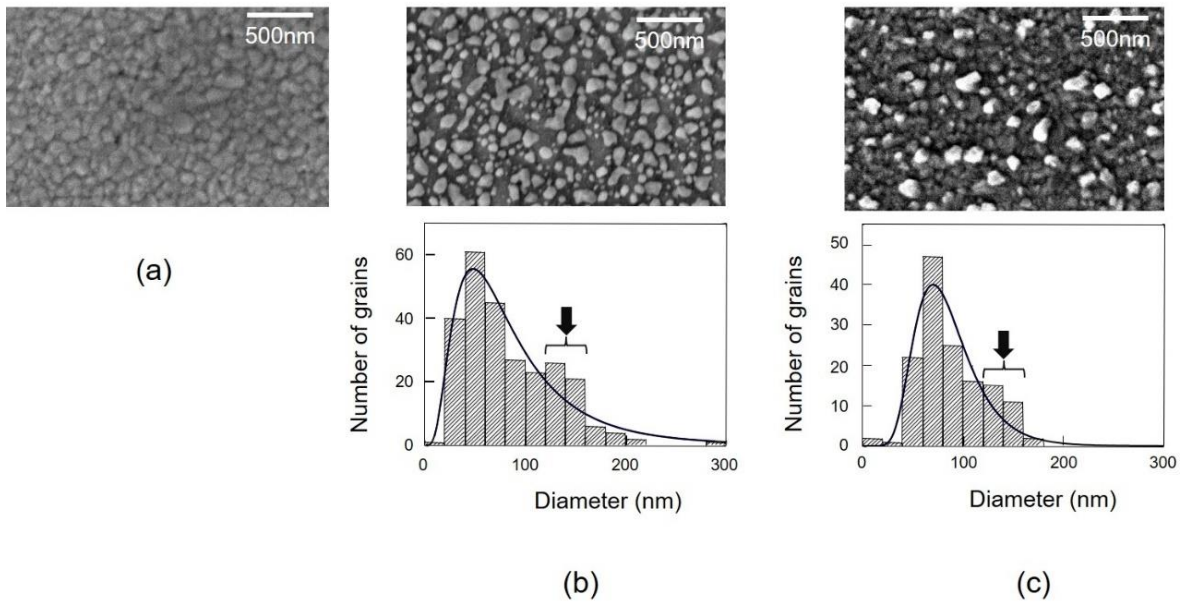

Fig. 4 Scanning electron microscopic images of Ag film surfaces.
(a), (b), and (c) show images of devices A, B, and C, respectively. Lower parts of (b) and (c) show histograms of the distribution of the Ag grain diameters. The downward arrows represent the bumps on the histograms.

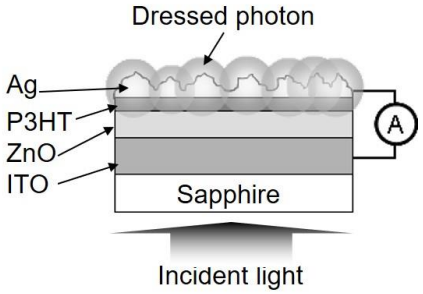

Fig. 5 Operation of the fabricated photovoltaic device.

Figure 6 shows the measured dependence of the generated photocurrent density on the irradiation light wavelength. The wavelength range of the measurement was 580–670 nm, which was longer than the wavelength λ_c (=570 nm) of the P3HT. Curve A in this figure shows a very

low photocurrent density generated from device A. Curves B and C are for devices B and C, respectively. They show that photocurrents were generated even with irradiation light wavelengths longer than λ_c.

Curve C has a peak at 620 nm*, clearly confirming the PB effect. Wavelength selectivity was not so clearly seen in curve B (device B) compared with curve C, because of the lower light power (50 mW) irradiated during the fabrication process for device B. The clear wavelength selectivity of curve C was due to the efficient creation of DPs by the higher irradiation power (70 mW).

(*) The peak wavelength (620 nm) of curve C was 40 nm shorter than the wavelength, λ_0 (=660 nm), of the irradiation light used in the fabrication process. This difference in wavelength originated from the DC Stark effect induced by the reverse bias voltage, V_b, applied during the fabrication process.

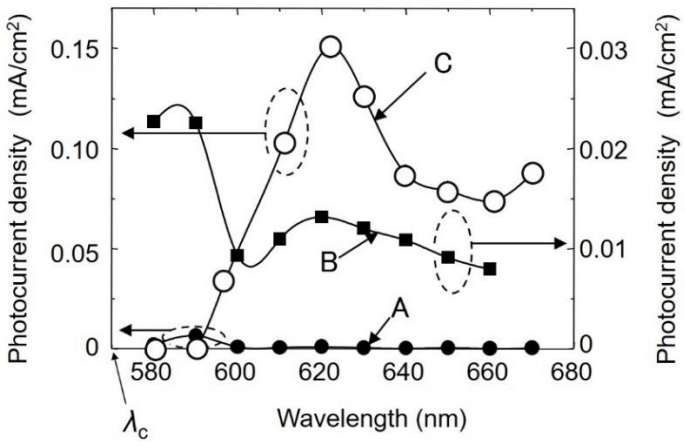

Fig.6 Relation between the incident light wavelength and the photocurrent density.
Curves A, B, and C represent the measured results for devices A, B, and C, respectively.

2.2 Light-emitting diodes using silicon crystals

This section reviews novel light-emitting diodes (LEDs) made of silicon (Si) crystal. Even though Si is an indirect-transition-type semiconductor, it emitted light due to the momentum exchange between a multi-mode coherent phonon in the DP and an electron in the conduction band of the Si. The details of the fabrication and operation of these LEDs have been described in [6-8]. They can be summarized as follows:

Fabrication

To fabricate an LED, as the first step, the surface of an n-type Si crystal was doped with boron (B) atoms to transform it to a p-type layer, thereby forming a pn-homojunction. As the second step, the crystal was annealed using a novel method named DP-assisted annealing [1,6]. This annealing process was:

(1) By means of current injection, the Si crystal was heated by Joule energy to diffuse the B atoms. During this heating, the Si crystal surface was irradiated with light (photon energy: $h\nu_{\text{anneal}}$) to create DPs at the B atoms.

(2) The electrons injected into the conduction band exchanged momenta with the phonons in the created DPs, thus recombining with positive holes and emitting light. This emission process was stimulated emission because it was triggered by the irradiation light.

(3) The emitted light propagated outside the Si crystal, which meant that a part of the Joule energy for heating was dissipated out in the form of optical energy. This dissipation locally cooled the region of the crystal at which the DP was created. As a result, the diffusion rate of the B atoms decreased locally.

(4) By means of a balance between heating by the Joule energy and cooling by the optical energy dissipation, the spatial distribution of B atoms varied autonomously and reached a stationary state.

Such a stationary distribution of B atoms could be the optimum for spontaneous emission because its probability was proportional to the probability of the stimulated emission in step **(2)** above.

Operation

The fabricated device emitted photons in response to current injection. The emitted photon energy $h\nu_{\text{em}}$ depended on $h\nu_{\text{anneal}}$ of the light irradiated during the DP-assisted annealing. From high-resolution analysis of the B atom distribution, it was found that two B atoms formed a pair whose length was n-times the lattice constant of the Si crystal. It was also found that the emitted photon energy $h\nu_{\text{em}}$ was equal to $E_{\text{g}} - nE_{\text{phonon}}$, where E_{g} and E_{phonon} are the bandgap energy of Si and the phonon energy, respectively. This formula indicates that the integer n, representing the length of the B atom pair as shown above, corresponds to the number of phonons that contributed to the momentum exchange with electrons for the photon emission. The emitted photon energy, $h\nu_{\text{em}}$, coincided with $h\nu_{\text{anneal}}$, an effect that is called the photon breeding (PB) effect.

2.3 Nano-droplets

Nano-droplets (NDs) are novel optical energy down-conversion devices that have been used to increase the conversion efficiency of solar cell batteries. The details of their fabrication and operation have been described in [9-13]. They can be summarized as follows:

Fabrication

Two kinds of nanometer-sized particles (NP1 and NP2) were dispersed into a liquid ultraviolet (UV)-setting resin. For example, a CdSe nano-crystal was used as NP1, while a ZnO or a CdS nano-crystal was used as NP2. Subsequently, the liquid was irradiated with visible light (photon energy: 2.33 eV) to create DPs selectively on the surface of NP1s. The energy of the created DP transferred to the neighboring equal-sized NP2s due to the size-dependent resonance of the DP momentum [9,14]. These NP2s created DPs whose energies were as high as the UV photon energy thanks to the contribution from the phonon energy in the DP. Finally, these DPs cured the liquid UV-setting resin around NP1 and NP2, resulting in the formation of an ND in which NP1 and NP2 were confined.

Operation

For operation, the fabricated ND was irradiated with UV light whose photon energy was tuned to the electron energy in NP2 in the ND (3.06 eV). Then, a DP was created on NP2, and its energy was transferred from NP2 to NP1, enabling visible light emission (2.08 eV) from NP1. This emission process corresponds to optical energy down-conversion.

3. Results of numerical simulations and associated problems

This section reviews numerical simulations that have been carried out for the three devices described in Section 2.

3.1 Photovoltaic devices having a silver electrode with a unique surface morphology

During the DP-assisted material formation process of a granular Ag film with a unique surface morphology, the photovoltaic device was open to the environment and thus involved energy flow and was subjected to environmental fluctuations. A two-dimensional nonequilibrium statistical mechanics model was used to describe the nonequilibrium dynamics [15]. In this model, it was assumed that two stochastic variables (i.e., the number of deposited Ag grains and the amount of electrical charge) dynamically coupled at each site of a two-dimensional square lattice and evolved with time.

The temporally varying magnitude of the repulsive Coulomb potential at each site caused by the charges was calculated in order to simulate the drift and deposition processes of Ag particles. The contribution of the DP was included by introducing irradiation light power b per site on the lattice. By regarding b as an external control parameter, it was shown that as b increased, a transition of the surface morphology occurred at a critical value b_c. That is, when $b \le b_c$, the DPs were not created effectively, and random Ag deposition was maintained as long as the simulation was continued (**State I**). When $b > b_c$, on the other hand, the DPs were created effectively, and Ag deposited autonomously, resulting in the formation of a unique surface morphology of the Ag film (**State II**). It was found that the transition from **State I** to **State II** was similar to the equilibrium second-order phase transitions.

As a result of this simulation, a configuration of Ag clusters on the surface was reproduced in the stationary state. Figure 7 shows the cluster size distribution in **State II**. As indicated by a downward arrow, a bump was found at size 11, which was consistent with the experimentally observed bumps identified by the downward arrows in Figs. 4(b) and (c). However, several problems were found with the simulation:

(p1-1) The maximum size of the DP was neglected even though it has been experimentally found [16].

(p1-2) The size-dependent resonance effect of the DP energy transfer was not correctly considered.

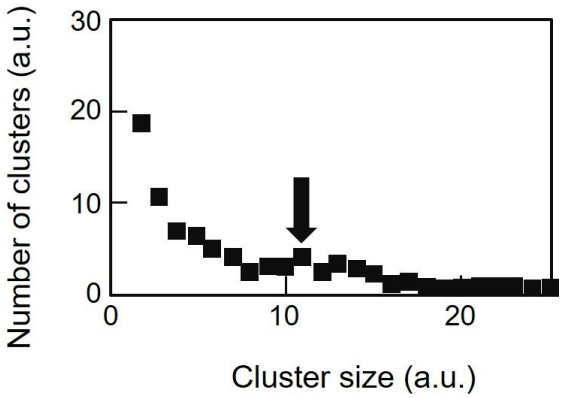

Fig.7 Relation between the size and the number of clusters in the steady state in state II.
The downward arrow represents a bump on this relation.

3.2 Light-emitting diodes using silicon crystals

The origin of the PB effect in the Si-LED was that the spatial distribution of B atoms played the role of genes. That is, this distribution bore the generic information and autonomously varied depending on the photon energy and polarization of the light irradiated during the DP-assisted annealing,

eventually reaching a stationary state. The stable spatial distribution of B atoms was reproduced, and the characteristics of the emitted light were simulated by a numerical simulation using a nonequilibrium statistical mechanical model [17].

For this simulation, a two-dimensional square lattice was assumed to represent the pn-junction in which the B atoms existed, and the thermally diffusing behavior of the B atoms was represented by a random walk of the B atoms on the lattice. By using an injected current, I, and an irradiation light power, P^0, as external control parameters, a simulation model composed of seven steps was formulated:

(Step 1) A random walk of B atoms forming B atom pairs with length d (=3a) on the square lattice was introduced, where a is the lattice constant of the Si crystal.

(Step 2) A random variable X was generated in order to represent the number of electrons for generating the Joule energy. Its distribution followed a Poisson process whose average was proportional to I.

(Step 3) Another random variable Y was generated that also followed a Poisson process. Its average was proportional to P, where P ($= P^0 + P^{PB}$) was the sum of the power, P^0, of the light irradiated during the DP-assisted annealing and the power, P^{PB}, of the emitted light. By adding the spontaneously emitted light power to Y, the total number of virtual photons Y^* ($= Y + 1$) that contributed to producing the PB effect was derived.

(Step 4) By means of the balance between the numbers of electrons and photons, being injected and irradiated during the DP-assisted annealing, respectively [7, 18], a value $Z = \min(X,Y^*)$ was derived to represent the number of photons created by the B atom pair.

(Step 5) By executing **Steps 1-4** for all the B atom pairs, the values Z were summed to represent the value P^{PB}.

(Step 6) In the case where $Z \geq 1$, the random walker was regarded as being inactivated. This was because the created photon with power P^{PB} propagated out from the Si crystal, and as a result, the thermal energy was lost. At that moment, the simulation was terminated.

(Step 7) In the case where $Z < 1$, the random walker was still active and hopped to the adjacent site, and the simulation was repeated by returning to **Step 1**.

The results obtained by the numerical simulation were as follows:

Fabrication

The regions A and B in Figure 8 show the temporal variation of the simulated power, P^{PB}, of the light emitted during the DP-assisted annealing [19]. In region A, the power increased immediately after the DP-assisted annealing started. Then it showed relaxation oscillation, such that the amplitude of the oscillation decreased with time. Subsequently, in region B, the power reached the stationary state after a certain time and showed a relatively small fluctuation.

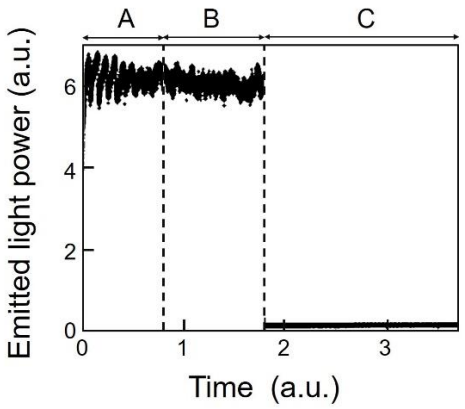

Fig. 8 Output power of photon emitted from the device.

The regions A and B represent the state of transition and a stationary state during the device fabrication. The region C is the output power emitted during the device operation. The values used for the simulations were I =40 and P^0 =80 in regions A and B. They were I =4 and P^0 =0 in region C.

Operation

Region C in Fig. 8 shows the power P^{PB} emitted during the device operation. Its value was smaller than those in regions A and B because of the smaller injection current than those injected for the DP-assisted annealing. However, it was stable over time. This was because the spatial distribution of the B atom pairs in the Si crystal was fixed, and random walks of the B atoms were suppressed.

The PB effect with respect to polarization has been also experimentally observed. In this effect, the polarization of the emitted light was equivalent to that of the light irradiated during the DP-assisted annealing [20]. Numerical simulations reproduced this effect by counting the number of created photon pairs that were orthogonally polarized. Here, it was assumed that the B atom pairs followed two independent Poisson distributions depending on the orientation of the B atom pairs on the square lattice.

Although the results of the numerical simulations above were consistent with most of the experimental results, several problems were found, including:

(p2-1) The simulation employed a two-dimensional model.

(p2-2) It was not straightforward to describe the details of the PB effect when using the conventional nonequilibrium statistical mechanical model, which relied on the temperature-dependent thermal diffusion. Novel models that incorporate theories of stochastic processes and quantum probability are required.

3.3 Nano-droplets

The experimental results in Section 2.3 have been analyzed by the following numerical simulations:

Fabrication

The numerical simulation confirmed that the rate of pairing NP1 and NP2 was **(1)** highest when their sizes were equal (Fig. 9(a)), and **(2)** higher when the liquid temperature was higher (Fig. 9(b)) [12]. Finding **(1)** originated from the size-dependent resonance of the DP momentum. Finding **(2)** was because the rate at which NP1 and NP2 encountered each other depended on the random walk velocity of the Brownian motion of the NPs in the liquid UV-setting resin. These two findings were consistent with the experimental results.

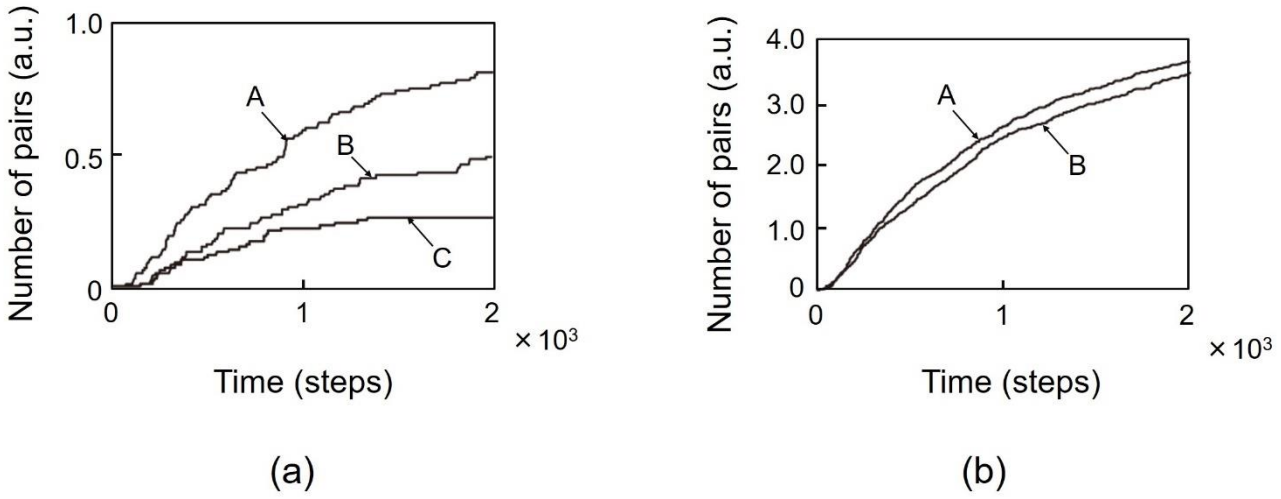

Fig.9 Temporal increases in the number of pairs (Fig. 7 in ref.[12]).

(a) Dependence on the ratio of the sizes a_{NP1} and a_{NP2} of the two NPs. The curves A, B, and C represent the results for a_{NP1} / a_{NP2} = 1, a_{NP1} / a_{NP2} < 1, and a_{NP1} / a_{NP2} > 1, respectively. (b) Dependence on the temperature of the liquid UV-setting resin. The curves A and B represent the results for high- and low-temperature liquids, respectively.

Operation

The validity of the present numerical simulation has been confirmed because the experimentally evaluated magnitude of the spectral peak shift of the light emitted from the CdSe (NP1) was consistent with the simulated temporal behavior of the NP-pair formation rate (Figs. 9(a) and (b)).

However, it should be pointed out that findings **(1)** and **(2)** above could be presumed by simply evaluating the experimental results. This means that the simulation was not essential for analyzing the experimental results. Furthermore, several problems were found with the simulation, including:

(p3-1) The simulation employed a one-dimensional model.

(p3-2) The simulation did not analyze the case of $N_2 / N_1 \neq 1$ (where $N_1 \gg 1$ and $N_2 \gg 1$) even though experiments have demonstrated that large numbers of NP1 ($N_1 \gg 1$) and NP2 ($N_2 \gg 1$) were confined in the fabricated NDs. Furthermore, their ratio N_2 / N_1 was not unity in the experiments.

(p3-3) The simulation did not introduce the deceleration of the Brownian motion of the NPs that originated from temporal hardening of the liquid UV-setting resin during the light irradiation.

(p3-4) The simulation did not introduce the recoiling of NP1 from NP2 that originated from the exchange of their momenta during the DP energy transfer.

4. Future directions

The essential feature, common to the fabrication process of the devices described in Sections 2.1 to 2.3 (devices 1–3, respectively), was that the spatial distributions of the DPs were autonomously optimized by means of the external control parameters in order to realize the largest contribution of the DPs to the device operation. As summarized in Table 2, these parameters increased the number of relevant NPs in device 1 during its fabrication, whereas they remained constant in devices 2 and 3. By referring to this table, problems in conventional numerical simulations and suggestions for solving them are presented in this section.

Table 2 Fabrication processes for the three devices.

	NPs used	Temporal variation of the number of the NPs	Motions of NPs	External control parameters
Device 1	Ag atoms	Increased	Depositing on the surfaces of Ag grains	Irradiated light and applied voltage
Device 2	B atoms	Maintained constant	Forming pairs	Irradiated light and injected current
Device 3	NP1 (made of CdSe), NP2 (made of ZnO or CdS)	Maintained constant	Pairing to form an ND	Irradiated light and resin temperature

4.1 Problems in conventional numerical simulations

The conventional numerical simulations relied on the theories of statistical mechanics and complex-system science, which are branches of traditional on-shell science. Although they succeeded in reproducing most of the experimental results, there were several problems that remain to be solved to explore future directions:

[1] In the conventional simulations, the numerical values were carefully selected in order to fit the results to the experimental results. However, the essential problem in these simulations was not a quantitative comparison with the experimental results, but identifying the origins of the DP creation and the autonomous energy transfer of the DP. That is, we need to answer the questions "What is the DP?" and "What are the intrinsic features of the DP?" The answers to these questions have not yet been given.

[2] The answer to the question "What is the nature of the interaction between nanometer-sized materials via the DP?" has not yet been given either. The absence of an answer originates in the intrinsic nature of on-shell science. One example was that even if infinite numbers of electromagnetic modes in the on-shell region were superposed, this superposition cannot represent the off-shell electromagnetic field that plays an essential role in the interaction. The off-shell field is unrelated to and completely different from the on-shell field. The problem is how to develop off-shell scientific theories that are indispensable for finding the answer to this question.

4.2 Suggestions for finding solution

Possible suggestions for finding the solutions described in the previous sections are:

{1} (To problem **[1]** in Section 4.1) A maximum size of the DP should be introduced to establish a three-dimensional model.

{2} (To problem **[2]** in Section 4.1) The concepts of "interaction" and "off-shell field" should be introduced.

{3} (For device 1; refer to **(p1-1)** and **(p1-2)** at the end of Section 3.1) It should be advantageous to introduce a function $\mathbf{1}(\alpha)$ in order to represent the maximum size of the DP, where

$$\mathbf{1}(\alpha)=\begin{cases}1 & ;\alpha \le \alpha_{\mathrm{DP\,max}} \\ 0 & ;\alpha > \alpha_{\mathrm{DP\,max}}\end{cases}$$

where $\alpha_{\mathrm{DP\,max}}$ is the maximum size of the DP. Experimental and theoretical values are 50–70 nm [16] and 38 nm [21], respectively. By using this function, the effective potential of the DP can be revised to $V_{\mathrm{eff,\,rev}}(r)=\mathbf{1}(\alpha)\cdot\exp(-r/\alpha)/r$.

{4} (For device 2; refer to **(p2-1)** and **(p2-2)** at the end of Section 3.2) A three-dimensional model should be established.

{5} (For device 3; refer to **(p3-1)** – **(p3-4)** at the end of Section 3.3) A theoretical expression for the size-dependent resonance should be introduced into the model.

Several discussions have been made recently by following suggestions **{1}**-**{5}** above, and

it has been suggested that it was advantageous to employ a quantum walk (QW) model in the numerical simulations for solving problems **[1]** and **[2]** in Section 4.1 [22]. This simulation is expected to give the answers for describing the off-shell scientific phenomena by developing a QW model with an infinite number of degrees of freedom. Based on this description, it is expected that it will be possible to find the origin of the interaction between the quantum fields by introducing a spacelike field into the QW model. The line-graph method [23] could be advantageously used for this. Furthermore, this method could succeed in introducing the phase of the Yukawa-type function (, the effective potential of the DP) to the simulation. This is expected to result in a description of the mechanical phenomena generated by the DP, such as the recoil effect[*][24,25], as discussed at the end of Section 3.3.

(*) It has been experimentally demonstrated that freely moving atoms in a vacuum were deflected or trapped by a DP.

5. Summary

The first part of this article presented experimental results on novel devices that were fabricated and operated by using dressed photons. These devices were photovoltaic devices having an Ag electrode with a unique surface morphology, light-emitting diodes using Si crystals, and nano-droplets in which pairs of nanometer-sized semiconductor particles were confined. The second part reviewed the results of numerical simulations for these devices by using a random walk model relying on statistical mechanics and complex-systems science. It also described the problems with these simulations and presented some suggestions for solving them. Finally, it was pointed out that a three-dimensional off-shell scientific model that takes account of the interaction in a nanometric space should be developed, and it was suggested that the line-graph method of the quantum walk model could be advantageously used.

Acknowledgements

The author thanks Prof. N. Tate (Kyushu Univ.) for his collaboration in the experimental and theoretical studies on nano-droplets.

References

[1] M. Ohtsu, *Dressed Photons* (Springer, 2014).

[2] M. Ohtsu, I. Ojima, and H. Sakuma, “Dressed Photon as an Off-Shell Quantum Field,” *Progress in Optics* Vol.64, (ed. T.D. Visser) pp.45-97 (Elsevier, 2019).

[3] M. Ohtsu, “Embarking on theoretical studies for off-shell science guided by dressed photons,” *Off-shell Archive* (November 2018) Offshell: 1811R.001.v1. **DOI** Offshell: 1811R.001.v1, http://offshell.rodrep.org/?p=176
[4] M. Ohtsu, “Indications from dressed photons to macroscopic systems based on hierarchy and autonomy,” *Off-shell Archive* (June, 2019) Offshell: 1906R.001.v1. **DOI** 10.14939/1906R.001.v1, http://offshell.rodrep.org/?p=201
[5] S. Yukutake, T. Kawazoe, T. Yatsui, W. Nomura, K. Kitamura, M. Ohtsu, “Selective photocurrent generation in the transparent wavelength range of a semiconductor photovoltaic device using a phonon-assisted optical near-field process,” *Appl. Phys.* B **99**, 415 (2010) pp. 415-422.
[6] M. Ohtsu, *Silicon Light-Emitting Diodes and Lasers* (2016, Springer).
[7] M. Ohtsu and T. Kawazoe, “Principles and Practices of Si Light Emitting Diodes using Dressed Photons,” *Off-shell Archive* (May 2018) Offshell: 1805R.001.v1. **DOI** Offshell: 1805R.001.v1, http://offshell.rodrep.org/?p=129
[8] M. Ohtsu and T. Kawazoe, “Principles and practices of Si light emitting diodes using dressed photons,” *Advanced Materials Letters*, **10** (2019) pp.860-867.
[9] M. Ohtsu, “Dressed photon phenomena that demand off-shell scientific theories,” *Off-shell Archive* (November 2019). Offshell: 1911R.001.v1. **DOI** Offshell: 1911R.001.v1, http://offshell.rodrep.org/?p=232
[10] N. Tate, Y. Liu, T. Kawazoe, M. Naruse, T. Yatsui, and M. Ohtsu, “Fixed-distance coupling and encapsulation of heterogeneous quantum dots using phonon-assisted photo-curing,” *Appl. Phys.* B, **110** (2013) pp.39-45.
[11] N. Tate, Y. Liu, T. Kawazoe, M. Naruse, T. Yatsui, and M. Ohtsu, “Nanophotonic droplet: a nanometric optical device consisting of size- and number-selective coupled quantum dots,” *Appl. Phys.* B, **110** (2013) pp.293-297.
[12] N. Tate, M. Naruse, Y. Liu, T. Kawazoe, T. Yatsui, and M. Ohtsu, “Experimental demonstration and stochastic modeling of autonomous formation of nanophotonic droplets,” *Appl. Phys.* B, **112** (2013) pp.587-592.
[13] N. Tate, W. Nomura, T. Kawazoe, and M. Ohtsu, “Novel wavelength conversion with nanophotonic droplet consisting of coupled quantum dots,”*Opt. Express*, **22** (2014) pp.10262-10269.
[14] S. Sangu, K. Kobayashi, and M. Ohtsu, “Optical near fields as photon-matter interacting systems,” *J. Microsc*. **202** (2001) pp.279-285.
[15] K. Takahashi, M. Katori, M. Naruse, and M. Ohtsu, *Appl. Phys.* B, **120** (2015) pp.247-254.
[16] M. Ohtsu and T. Kawazoe, “Experimental estimation of the maximum size of a dressed photon,” *Off-shell Archive* (February 2018) Offshell: 1802R.001.v1. **DOI** 1802R.001.v1, http://offshell.rodrep.org/?p=98
[17] M. Katori and H. Kobayashi, in *Prog. Nanophotonics* 4 (ed. by M. Ohtsu and T. Yatsui) (Springer, Heidelberg, 2017) pp.19-55.
[18] J. H. Kim, T. Kawazoe, and M. Ohtsu, “Optimization of dressed-photon—phonon-assisted annealing for fabricating GaP light-emitting diodes,” *Appl. Phys*. A **121** (2015) pp.1395-1401.
[19] M. Ohtsu and M. Katori, “Complex System of Dressed Photons and Applications,” *The Review of Laser Engineering*, **45** (2017) pp.139-143 (in Japanese).
[20] T. Kawazoe, K. Nishioka, and M. Ohtsu, “Polarization control of an infrared silicon light-emitting diode by dressed photons and analyses of the spatial distribution of doped boron atoms,” *Appl. Phys.*A, **121** (2015) pp.1409-1415.

[21] H. Sakuma, “On the problem of quantization of Clebsch dual field and a quantized representation of dressed photon,” *Proc. of the Workshop on Basic Mathematic-Physical Studies on Dressed Photon* (ed. by T. Takiguchi), *Mathematics for Industry Research* No.14, Inst. Mathematics for Industry, Kyushu Univ., (February 2019) pp.127-148.
[22] H. Saigo, “Dressed Photon and Quantum Walk,” *Abstracts of the 66th Jpn. Soc. Appl. Phys. Spring Meeting*, March 2019, Tokyo, Japan, paper number 10p-W621-13.
[23] E. Segawa, S. Sangu, and M. Ohtsu, “An expression for dressed photon by quantum walks on line graphs,” *Abstracts of the 80th Jpn. Soc. Appl. Phys. Spring Meeting*, September 2019, Sapporo, Japan, paper number 19p-E314-5.
[24] H. Ito, T. Nakata, K. Sakaki, and M. Ohtsu, “Laser Spectroscopy of Atoms Guided by Evanescent Waves in Micron-Sized Hollow Optical Fibers,” *Phys. Rev. Lett.* **76** (1996) pp.4500-4503.
[25] M. Ohtsu, “Near-Field Optical Atom Manipulation: Toward Atom Photonics,” Chapter 11 in *Near-Field Nano/Atom Optics and Technology*, (Springer, Tokyo, 1998) pp.217-266.